Real-time NIR-II Fluorescence Imaging-Guided Precision Thrombolysis with a Molecularly Planarized Phototheranostic Agent

Guosheng Zhang[1,3], Leilei Si[1,2], Fuhai Zhou[1,2], Xiaofang Song[1,2] and Hongming Wang[1,2]

[1] Jiangxi Provincial Key Laboratory of Functional Crystalline Materials Chemistry, Nanchang 330031, China.

[2] College of Chemistry and Chemical Engineering, Nanchang University, Nanchang 330031, China

[3] Information Engineering College, Nanchang University, Nanchang 330031, China

Corresponding author: Hongming Wang, PhD, Jiangxi Provincial Key Laboratory of Functional Crystalline Materials Chemistry, Nanchang 330031, China

E-mail: hongmingwang@ncu.edu.cn

Materials

All chemical intermediates used in this study were purchased from Energy Chemical. All solvents were obtained from Sinopharm Chemical Reagent Co., Ltd. and were of analytical grade. With the exception of tetrahydrofuran (THF), no further purification was performed for other reagents. THF was redistilled prior to use to remove residual water. Reagents for biological assays were sourced from multiple suppliers. DSPE-PEG_{2000} was acquired from Ponsure Biotechnology, and HUVEC cells were kindly provided by the Cell Bank of the Chinese Academy of Sciences. Phosphate-buffered saline (PBS), Dulbecco's Modified Eagle Medium (DMEM), and Calcein-AM/Propidium Iodide (PI) were purchased from Wuhan Servicebio Technology Co., Ltd. The Annexin V-FITC/PI Apoptosis Kit was procured from KeyGen Biotech Co., Ltd.

Measurement

^{1}H and ^{13}C NMR spectra were recorded on an AVANCE III HD 400 MHz spectrometer (Bruker, Germany). High-resolution mass spectrometry (HRMS) data were obtained using a UHPLC30A-Trip TOF 5600+ system (SCIEX, Japan). UV-Vis-NIR absorption spectra were measured with a Lambda 750 spectrophotometer (PerkinElmer, USA). NIR-II fluorescence spectra were acquired on an FLS 1000 steady-state and lifetime fluorescence spectrometer (Edinburgh Instruments, UK). Single-crystal X-ray diffraction (XRD) data were collected on a Bruker Smart Apex diffractometer (Bruker, Germany). The morphology of the nanoparticles was examined by transmission electron microscopy (TEM) (JEOL, Japan). Dynamic light scattering (DLS) and zeta potential analyses of the nanoparticles were performed on a Mastersizer 3000 system (Malvern Instruments, UK). The excitation laser was purchased from Changchun New Industries Optoelectronics Technology Co., Ltd. (CNI, model: MIL-S-1064) and coupled with an FLIR E76 thermal imaging camera (FLIR, USA) to monitor the photothermal performance. Fluorescence imaging data in the NIR-II window were captured using a NIR-II imaging system equipped with an InGaAs camera, which was procured from Artemis Intelligent Imaging (MARS, China).

Synthesis and Characterization of Compounds

The synthesis routes of SQ-BiPh and SQ-BiPh-S are as shown in the scheme. The structures of both compounds were confirmed by ^{1}H NMR, $^{13}CNMR$, and mass spectrometry (MS). The synthesis was carried out according to previously reported literature procedures[1].

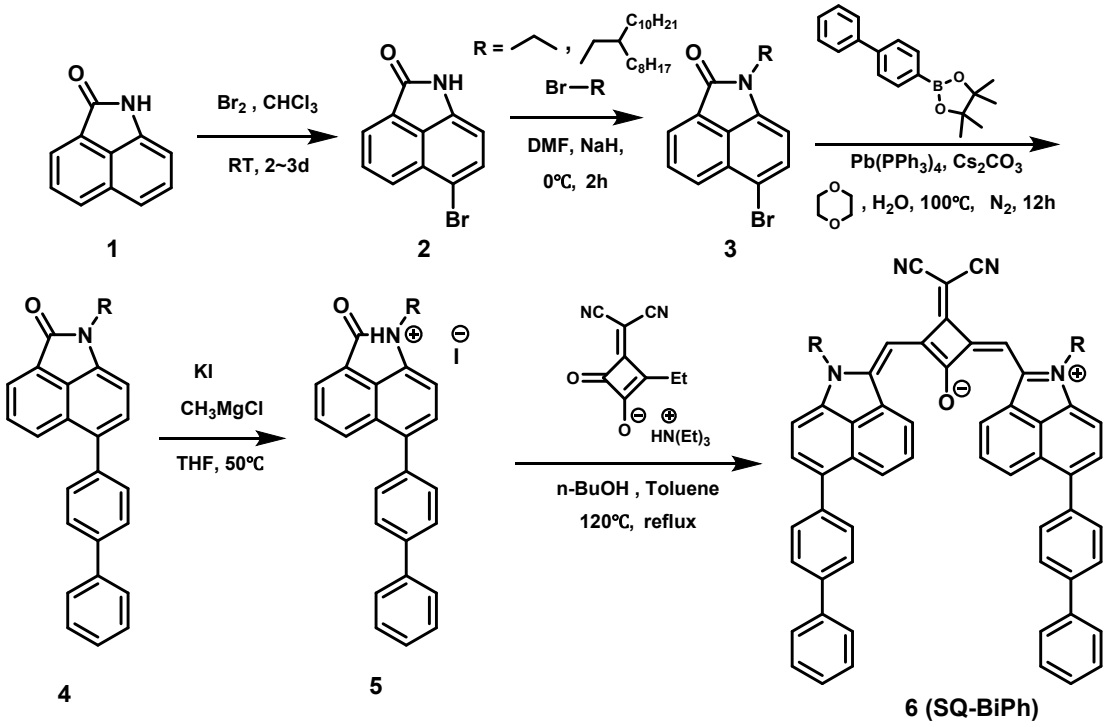

Figure S1. Synthesis routine of SQ-BiPh.

Synthesis of Compound 2: Compound 1 (10 mmol, 1.69 g) was dissolved in $CHCl_3$ and stirred in an ice bath at 0 °C for 5-10 minutes. Liquid bromine (15 mmol, 2.36 g) was then added dropwise. The reaction mixture was stirred for 2-3 days. After quenching the reaction with saturated sodium thiosulfate solution, the product was extracted with ethyl acetate and brine. The combined organic layers were dried over sodium sulfate, filtered, and concentrated under reduced pressure to afford the crude product. Purification by silica gel column chromatography (petroleum ether/ethyl acetate = 50 : 1) yielded Compound 2 (2.10 g, 85.3% yield).^{1}H NMR (400 MHz, DMSO-d_6) δ 10.87 (s, 1H), 8.07 (dd, J = 7.7, 1.6 Hz, 2H), 7.93 - 7.86 (m, 1H), 7.71 (d, J = 7.5 Hz, 1H), 6.88 (d, J = 7.6 Hz, 1H). ^{13}C NMR (151 MHz, DMSO-d_6) δ 168.66, 138.56, 132.30, 130.84, 129.96, 128.79, 127.80, 127.10, 125.25, 112.35, 107.92, 40.53, 40.41, 40.27, 40.14, 40.00, 39.86, 39.72, 39.58. TOF-MS m/z: calculated $C_{11}H_6BrNO$ (m/z):246.9533, found:245.9560.

Synthesis of Compound 3: Compound 2 (10 mmol, 2.46 g) was dissolved in dry DMF and stirred in an ice bath at 0 °C for 10 minutes. Sodium hydride (NaH, 60 mmol, 1.44

g) was then added portionwise slowly. The reaction mixture was stirred at room temperature for 0.5 hours. Subsequently, 9-(bromomethyl)nonadecane (15 mmol, 5.42 g) was introduced, and the reaction was continued at room temperature for 2 hours. The reaction was quenched with water, and the product was extracted with ethyl acetate and brine. The combined organic layers were dried over anhydrous sodium sulfate, filtered, and concentrated under reduced pressure to afford the crude product. Purification by silica gel column chromatography (petroleum ether/ethyl acetate = 25 : 1) yielded Compound 3 (5.29 g, 86.4% yield). ^{1}H NMR (400 MHz, $CDCl_3$) δ 8.06 (dd, J = 12.8, 7.6 Hz, 2H), 7.74 (dd, J = 8.3, 7.0 Hz, 1H), 7.60 (d, J = 7.6 Hz, 1H), 6.69 (d, J = 7.5 Hz, 1H), 3.74 (d, J = 7.4 Hz, 2H), 1.98 - 1.87 (m, 1H), 1.33 (p, J = 7.3 Hz, 8H), 1.27 - 1.18 (m, 24H), 0.85 (td, J = 6.9, 5.4 Hz, 6H). ^{13}C NMR (101 MHz, $CDCl_3$) δ 166.60, 138.58, 130.06, 129.07, 128.54, 127.73, 125.78, 124.99, 123.98, 112.76, 105.10, 76.35, 76.03, 75.71, 43.68, 37.92, 36.21, 30.88, 30.84, 30.51, 29.89, 29.07, 28.92, 28.59, 28.55, 28.50, 28.31, 28.25, 25.87, 25.45, 21.67, 21.63, 13.12, 13.10. TOF-MS m/z: calculated $C_{31}H_{46}BrNO$ (m/z):527.2863, found:528.2828.

Synthesis of Compound 4: Compound 3 (2.5 mmol, 1.32 g), 4-biphenylboronic acid pinacol ester (3 mmol, 0.84 g), cesium carbonate (12.5 mmol, 4.07 g), and tetrakis(triphenylphosphine)palladium(0) (0.25 mmol, 0.28 g) were added to 1,4-dioxane/water (100 mL, 10:1, v/v). The mixture was stirred at 100 °C under nitrogen for 12 h and then cooled to room temperature. The solvent was evaporated under reduced pressure. The residue was extracted with ethyl acetate and water. The organic layer was dried over anhydrous sodium sulfate, filtered, and concentrated under vacuum. The crude product was purified by silica gel column chromatography (petroleum ether/ethyl acetate = 30:1) to give compound 4 (2.45 g, 91.0% yield). ^{1}H NMR (400 MHz, $CDCl_3$) δ 8.21 (d, J = 8.2 Hz, 1H), 8.11 (d, J = 6.9 Hz, 1H), 7.76 (d, J = 2.0 Hz, 1H), 7.73 (d, J = 9.8 Hz, 2H), 7.70 (dd, J = 8.3, 1.3 Hz, 2H), 7.64 (d, J = 8.6 Hz, 2H), 7.50 (t, J = 7.5 Hz, 3H), 7.39 (t, J = 7.4 Hz, 1H), 6.98 (d, J = 7.3 Hz, 1H), 3.85 (d, J = 7.5 Hz, 2H), 2.12 - 1.94 (m, 1H), 1.41 - 1.20 (m, 32H), 0.87 (td, J = 7.0, 3.2 Hz, 6H). ^{13}C NMR (101 MHz, $CDCl_3$) δ 168.52, 140.77, 140.32, 139.60, 138.27, 133.71, 130.32, 130.01, 129.02, 128.95, 128.73, 127.79, 127.59, 127.45, 127.23, 127.08, 125.54, 124.49, 105.55, 77.48, 77.37, 77.16, 76.84, 44.89, 37.58, 32.05, 32.02, 31.88, 31.74, 30.14, 29.84, 29.77, 29.70, 29.48, 29.43, 26.68, 25.00, 22.83, 22.80, 14.27. TOF-MS m/z: calculated $C_{43}H_{55}BNO$ (m/z):601.4384, found:602.4358.

Synthesis of Compound 5: To a solution of compound 4 (2.28 mmol, 1.37 g) in anhydrous THF (20 mL) at 0 °C was added methylmagnesium chloride (5 mL, 3 M in THF, 15 mmol). The reaction mixture was heated to 50 °C and stirred for 2 h. After cooling to 0 °C, water (0.5 mL) and a saturated potassium iodide solution (70%, 4 mL)

were added. The resulting dark purple solution was extracted with dichloromethane and water. The organic layer was dried over anhydrous sodium sulfate and filtered. The solvent was removed under reduced pressure to afford the crude product of compound 5 (1.41 g), which was used directly in the next step without further purification.

Synthesis of Compound 6 (SQ-BiPh): A solution of compound 5 (2.30 mmol, 1.67 g) and compound 7 (1.15 mmol, 0.27 g) in toluene (10 mL) and n-butanol (10 mL) was refluxed for 2 hours using a Dean-Stark apparatus. After completion of the reaction, the mixture was concentrated under reduced pressure and purified by silica gel column chromatography (petroleum ether/ethyl acetate = 5:1) to afford compound 6.^{1}H NMR (600 MHz, $CDCl_3$) δ 8.64 (d, J = 7.3 Hz, 2H), 8.20 (d, J = 8.2 Hz, 2H), 7.84 (t, J = 7.8 Hz, 2H), 7.73 (d, J = 8.2 Hz, 4H), 7.69 - 7.62 (m, 8H), 7.58 (d, J = 7.5 Hz, 2H), 7.49 (t, J = 7.6 Hz, 4H), 7.42 - 7.38 (m, 2H), 7.18 (d, J = 7.6 Hz, 2H), 6.76 (s, 2H), 4.06 (d, J = 7.7 Hz, 4H), 2.18 (dt, J = 13.7, 6.9 Hz, 2H), 1.47 - 1.39 (m, 12H), 1.32 - 1.21 (m, 52H), 0.89 - 0.85 (m, 12H). ^{13}C NMR (151 MHz, $CDCl_3$) δ 174.12, 167.66, 163.27, 151.89, 141.04, 140.47, 140.45, 137.80, 135.98, 131.55, 130.44, 130.02, 129.82, 129.74, 128.95, 127.97, 127.60, 127.36, 127.07, 125.61, 118.10, 108.97, 94.24, 77.29, 77.08, 76.87, 49.06, 44.23, 38.00, 31.95, 31.91, 31.54, 31.43, 30.18, 30.03, 29.74, 29.69, 29.66, 29.62, 29.57, 29.39, 29.34, 26.42, 22.72, 22.70, 14.15, 1.06. TOF-MS m/z: calculated $C_{95}H_{112}N_4O$ (m/z):1325.8836, found:1325.8901.

Calculation of fluorescence quantum yield

Ground-state structure optimization and frequency calculations for the single SQ-BiPh molecule were performed using the Gaussian 09 (Revision D.01) software package with the density functional theory (DFT) method at the BLYP/6-311G(d,p) level. The frontier molecular orbitals and energy levels were derived from the optimized geometry of the single molecule. To determine the oscillator strength of the $S_0 \rightarrow S_1$ transition, time-dependent density functional theory (TD-DFT) calculations were carried out at the BLYP/6-31G(d,p) level under the IEFPCM solvation model based on the optimized structure[2].

Determination of NIR-II quantum yield

This study employed a (NIR-II) fluorescence quantum yield (ΦF) measurement method analogous to that reported in the literature, using IR-1061 dye (with a known ΦF of 0.182%) as the reference standard[3-4]. A series of IR-1061 solutions at varying concentrations were prepared in dichloromethane (DCM), with their absorbance at 1064 nm adjusted to approximately 0.10, 0.08, 0.06, 0.04, and 0.02. The fluorescence

spectra of these solutions were then recorded within the 1000-1300 nm wavelength range, and their integrated fluorescence intensities were calculated. A standard calibration curve for IR-1061 was obtained by performing a linear fit between the integrated fluorescence intensities and their corresponding absorbance values. For the SQ-BiPh NPs aqueous dispersions under investigation, fluorescence spectra were measured and integrated intensities calculated under identical experimental and data processing conditions, enabling the construction of the standard curve for SQ-BiPh NPs. The quantum yield ΦF was calculated using the following equation:

$$\Phi F_{NPs} = \Phi F_{ref} \frac{Slope_{NPs}}{Slope_{ref}} \frac{n_{H2O}^2}{n_{DCM}^2}$$

Here, $slope_{NPs}$ and $slope_{ref}$ represent the slopes of the calibration curves for SQ-BiPh nanoparticles and IR-1061, respectively. n_{sample} and n_{ref} denote the refractive indices of the sample solvent (water) and reference solvent (dichloromethane, DCM), respectively, with values of n_{H2O}=1.333 and n_{DCM}=1.417.

Photothermal properties of SQ-BiPh NPs

In this study, the photothermal performance of SQ-BiPh NPs was systematically evaluated under precisely controlled experimental conditions. A series of aqueous dispersions of SQ-BiPh NPs were prepared at concentrations of 0、5、10、20、50 and 100 μM. Under 1064 nm laser irradiation (1.0 W/cm^2), the temperature of each dispersion was monitored in real time to obtain time-dependent temperature profiles, thereby characterizing the concentration-dependent photothermal response. Additionally, SQ-BiPh NPs were subjected to cyclic irradiation using the same 1064 nm laser (1.0 W/cm²) with a 4-minute irradiation period followed by natural cooling to room temperature. Complete heating-cooling cycles were recorded, and photothermal stability was confirmed over six consecutive cycles. The photothermal conversion efficiency was calculated following established literature methods[5].

$$\boldsymbol{\eta} = \frac{hA\,(\Delta T_{Max,NPs} - \Delta T_{Max,H_2O})}{I(1 - 10^{-A_{1064}})}$$

In the above equation, **h** represents the heat transfer coefficient, and **A** denotes the

surface area of the sample holder. $\Delta T_{max,NPs}$ corresponds to the temperature change of the nanoparticles from the maximum steady-state temperature to room temperature, while $\Delta T_{max,H2O}$ refers to the analogous temperature change for pure water. ***I*** indicates the laser power density (1.0 W/cm²), and $\mathbf{A_{1064}}$ is the absorbance of the sample at 1064 nm. The product **hA** is determined by the following equation:

$$hA = \frac{m_D c_D}{\tau_s}$$

where m_D is the mass of pure water (0.15 g), and c_D is the specific heat capacity of pure water (4.2 $J \cdot g^{-1}$). The time constant τ_s was calculated using the following equation:

$$t = -\tau_s \, ln\left(\frac{T - T_{surr}}{T_{max} - T_{surr}}\right)$$

Here, T and t represent the real-time temperature and corresponding time during the cooling phase, respectively. T_{surr} and T_{max} denote the ambient temperature and the maximum plateau temperature, respectively.

Cell culture and cytotoxicity test

HUVEC cells were cultured at 37 °C in a humidified atmosphere containing 5% CO_2 and 95% air, using a complete endothelial cell-specific medium (e.g., EGM-2) supplemented with 1% antibiotics (penicillin and streptomycin). Cells were uniformly seeded at a density of 1×10^4 cells per well in gelatin-coated 96-well plates and allowed to grow for 24 h. Thereafter, the cells were treated with SQ-BiPh NPs at various concentrations for a further 24 h. After treatment, the medium was gently replaced with pre-warmed 1× PBS to wash the cells. Subsequently, 100 μL of a working solution prepared by mixing fresh endothelial cell medium and CCK-8 solution at a 10:1 ratio was added to each well, followed by light-protected incubation for 1-4 h. To determine cell viability, the absorbance at 450 nm was measured using a microplate reader after shaking the plate for 2 minutes.

NIR-II vascular fluorescence imaging

BALB/c-cJGpt mice were anesthetized with isoflurane and depilated before intravenous injection of SQ-BiPh nanoparticles (NPs) (200 μL, 80 μM) via the tail vein. Whole-body vascular fluorescence imaging was conducted post-injection using the wide-field mode of a NIR-II imaging system. Subsequently, the imaging mode was switched to posture-specific scanning to capture fluorescence images of the vasculature in the hind limbs and abdominal regions. Imaging data were acquired with an InGaAs camera, and imaging performance was optimized by adjusting long-pass filters, exposure times, and laser power. The collected fluorescence images were processed and analyzed using ImageJ software.

Hemolysis assay

The hemolysis assay was conducted to evaluate the hemolytic potential of SQ-BiPh NPs, following a previously reported method with minor modifications[6]. Briefly, blood was collected from healthy BALB/c mice and centrifuged at 2000 rpm to separate the serum. After carefully removing the serum with a syringe, the erythrocytes were washed five times with 1× phosphate-buffered saline (PBS) and resuspended in PBS. Then, 0.2 mL of the red blood cell suspension was mixed with 0.8 mL of various test solutions: ultrapure water as the positive control, PBS as the negative control, and SQ-BiPh NPs at different concentrations (dispersed in PBS) as the test groups. The mixtures were gently rotated and incubated at 37 °C for 2 hours. After incubation, the samples were centrifuged at 15,000 rpm for 10 minutes, and the absorbance of the supernatant was measured at 540 nm using a microplate reader to quantify the degree of hemolysis.

Animal experiments

The animal experimental protocol for this study was approved by the Institutional Animal Care and Use Committee (IACUC) of Nanchang University (Approval No. NCULAE-20230610005). All experimental procedures were conducted in strict accordance with national regulations and international guidelines for animal research. The BALB/c-Nude mice (approximately 20 g, n=20) and BALB/c mice (approximately 18 g, n=15) used in this study were supplied by Jiangsu GemPharmatech Co., Ltd.

(Jiangsu, China).

Clot formation

A 3 mL blood sample was collected from healthy mice and transferred into a centrifuge tube, where it was incubated undisturbed at 4 °C for 24 hours to facilitate natural coagulation. The formed clot was then uniformly sectioned into small pieces and further incubated at room temperature for 24 hours to enhance clot stabilization. Subsequently, the clots were thoroughly washed six times with phosphate-buffered saline (PBS) to remove residual blood cells and soluble impurities, resulting in a structurally stable in vitro thrombus model[7].

Mouse thrombus model

Femoral artery thrombosis was induced in female BALB/c mice using the $FeCl_3$ injury model, following an established literature method[8]. In brief, the mice were anesthetized, and the hair on their hind limbs was removed with a depilatory cream to fully expose the surgical area. The femoral arteries on both sides were exposed by careful dissection of the overlying skin. To induce thrombosis on the right side, a piece of filter paper was placed on the femoral artery to absorb interstitial fluid, followed by topical application of 10% ferric chloride ($FeCl_3$) solution for 10 minutes. After the induction period, the $FeCl_3$ solution was thoroughly removed, and the surgical site was rinsed with physiological saline. The left femoral artery was left untreated and served as the internal control.

Blood Hematology and Pathology Analysis

To evaluate the overall health status of the mice, blood samples were collected from different control groups before and after treatment. These samples were centrifuged to separate plasma, followed by analysis of hematological and biochemical parameters. Additionally, tissues and major organs were collected from the different control groups before and after treatment. These samples were promptly fixed in 4% formaldehyde solution. After fixation, 10 μm tissue sections were prepared for hematoxylin and eosin (H&E) staining for further pathological evaluation.

Table S1 Crystal data and structure refinement for SQ-H-S,SQ-Ph-S and SQ-BiPh-S[9].

Compound	**SQ-H-S**	**SQ-Ph-S**	**SQ-BiPh-S**
CCDC	2386554	2386555	2472690
Empirical formula	$C_{35}H_{23}N_4O$	$C_{48}H_{34}Cl_2N_4O$	$C_{60}H_{42}Cl_2N_4O$
Formula weight/g mol^{-1}	515.57	753.69	905.87
Temperature/K	193	193	190
Crystal system	monoclinic	monoclinic	monoclinic
Space group	Pc	$P2_1/n$	$P2_1/c$
a/Å	7.5098(11)	9.6814(4)	9.8352(6)
b/Å	22.374(3)	26.6549(11)	32.229(2)
c/Å	15.207(3)	15.0711(6)	14.8500(9)
α/°	90	90	90
β/°	93.623(6)	108.712(2)	105.319(5)
γ/°	90	90	90
Volume/Å^3	2550.1(7)	3683.6(3)	4539.8(5)
Z	4	4	4
ρ_{calc} g/cm^3	1.343	1.359	1.325
μ/mm^{-1}	0.415	1.273	1.665
F (000)	1076	1568	1888
Radiation	GaKα (λ = 1.34139)	GaKα (λ = 1.34139)	GaKα (λ = 1.34139)
Reflections collected	5387	20441	34459

Goodness-of-fit on F^2	1.031	1.033	1.043
Final R indexes [I≥2σ (I)]	R_1 = 0.1182, wR_2 = 0.2698	R_1 = 0.0497, wR_2 = 0.1126	R_1 = 0.0984, wR_2 = 0.2562
Final R indexes [all data]	R_1 = 0.2142, wR_2 = 0.3513	R_1 = 0.1130, wR_2 = 0.1392	R_1 = 0.1436, wR_2 = 0.2865

Table S2 Summary of reported NIR-II-emissive dye molecules for thrombus treatment.

Compound	**NPs Abs/Em [nm]**	**PLQY [%]**	**PTT [%]**	**Ref.**
TPNs/ICG-cRGD	808/830	-	-	[6]
Pkr(IR-Ca)Pda-uPA-cRGD	1048/1070	-	-	[10]
B@SP-C NPs	1200/-	0.08	73	[8]
4THTPB	732/1058	3.2	87.6	[7]
MTQPL-Arg@RGD NPs	800/1096	-	61.3	[11]
5SGNPs	820/1218	-	-	[12]
PSA@ADT-OH	660/780	-	40	[13]
SQ-BiPh NPs	1065/1131	0.274	39.7	This Work

Table S3 SQ-H、SQ-Ph、SQ-BiPh photophysical properties[9].

Compound	λ_{abs}[nm]	λ_{em}[nm]	ε_{1064nm}[$M^{-1}cm^{-1}$]	$\Phi_{NIR\text{-}II}$[%][a]	η[%]
SQ-H	946	1001	2140	/	/
SQ-Ph	980	1045	5786	/	/
SQ-BiPh	990	1035	5927	/	/
SQ-H NPs	959	1035	12955	0.09	57.5
SQ-Ph NPs	1065	1131	97840	4.22	48.3
SQ-BiPh NPs	1087	1131	107925	0.274	39.7

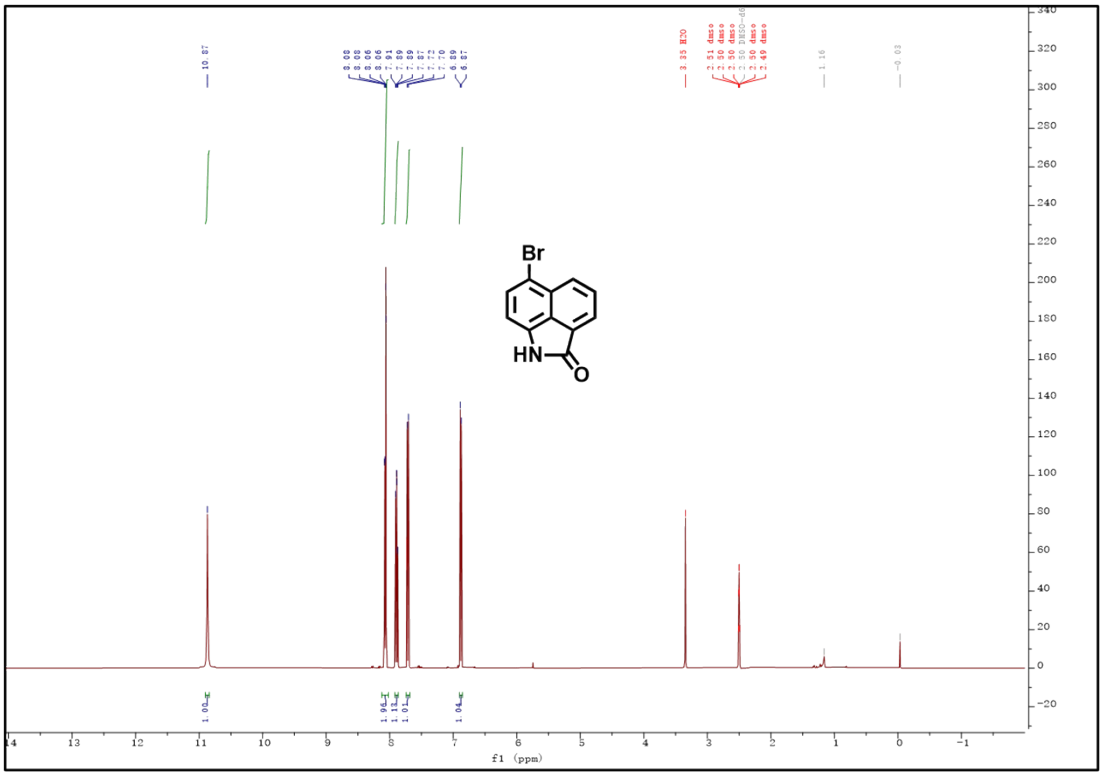
Br
HN
O
f1 (ppm)

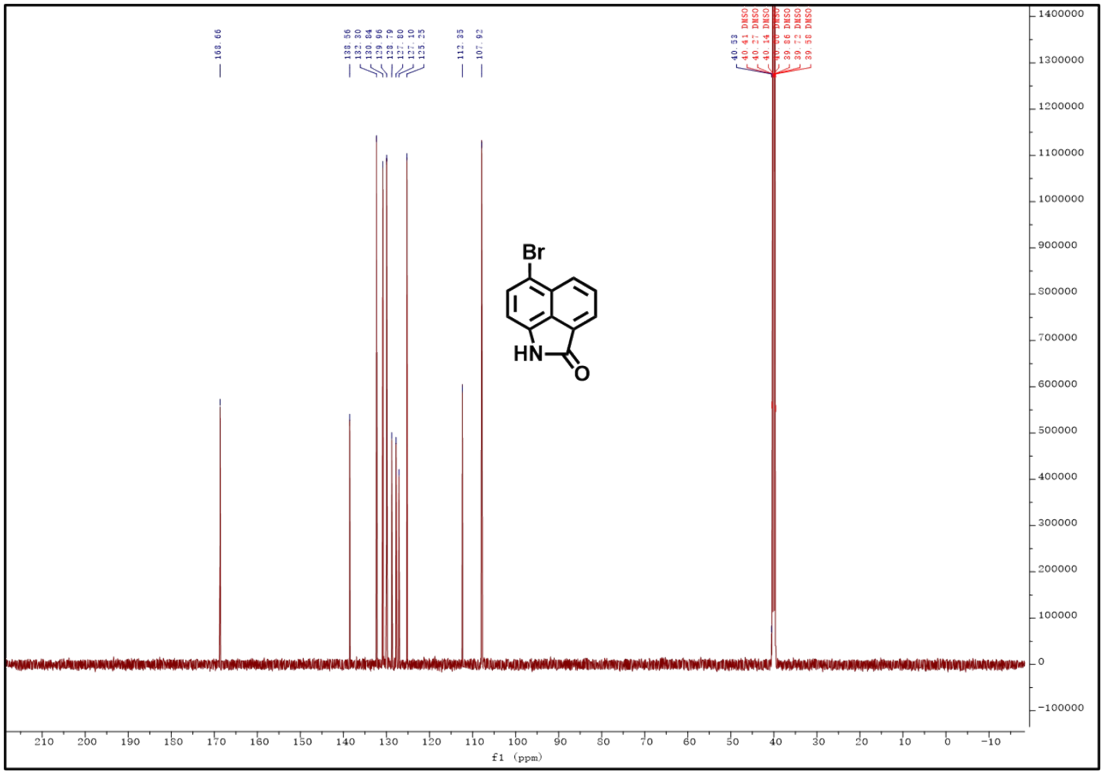
Br
HN
O
f1 (ppm)

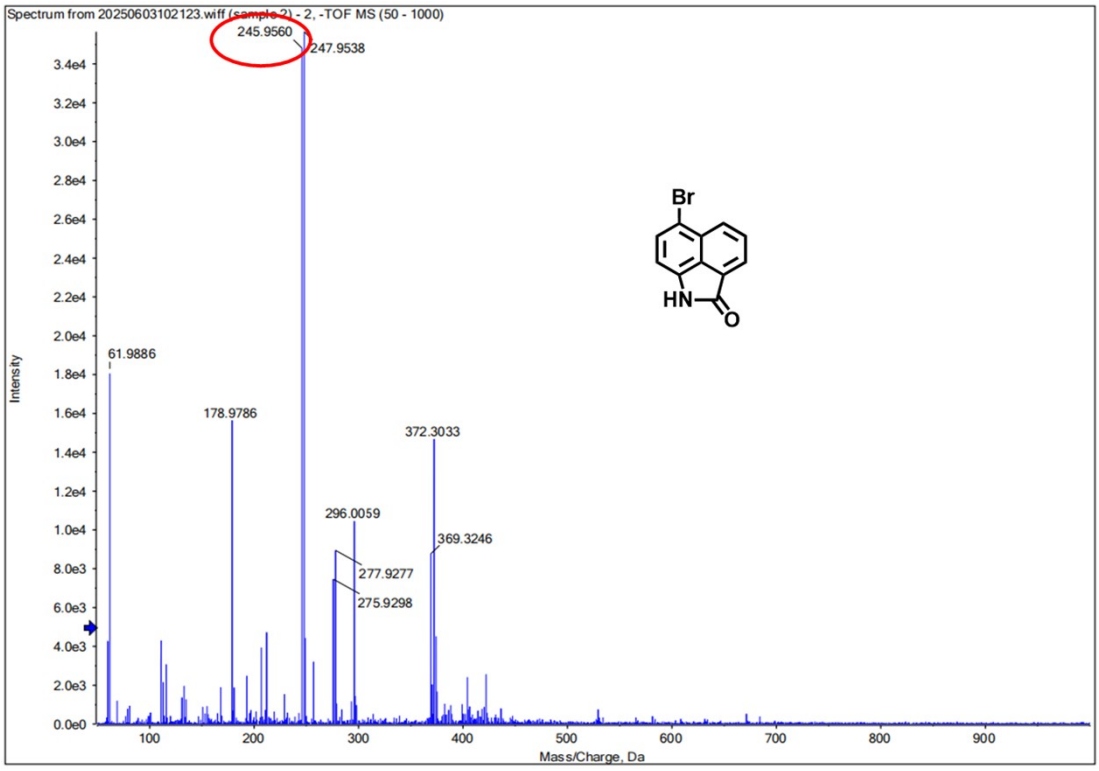

Figure S2. ^{1}H NMR, ^{13}C NMR, and TOF-MS spectra of compound 2.

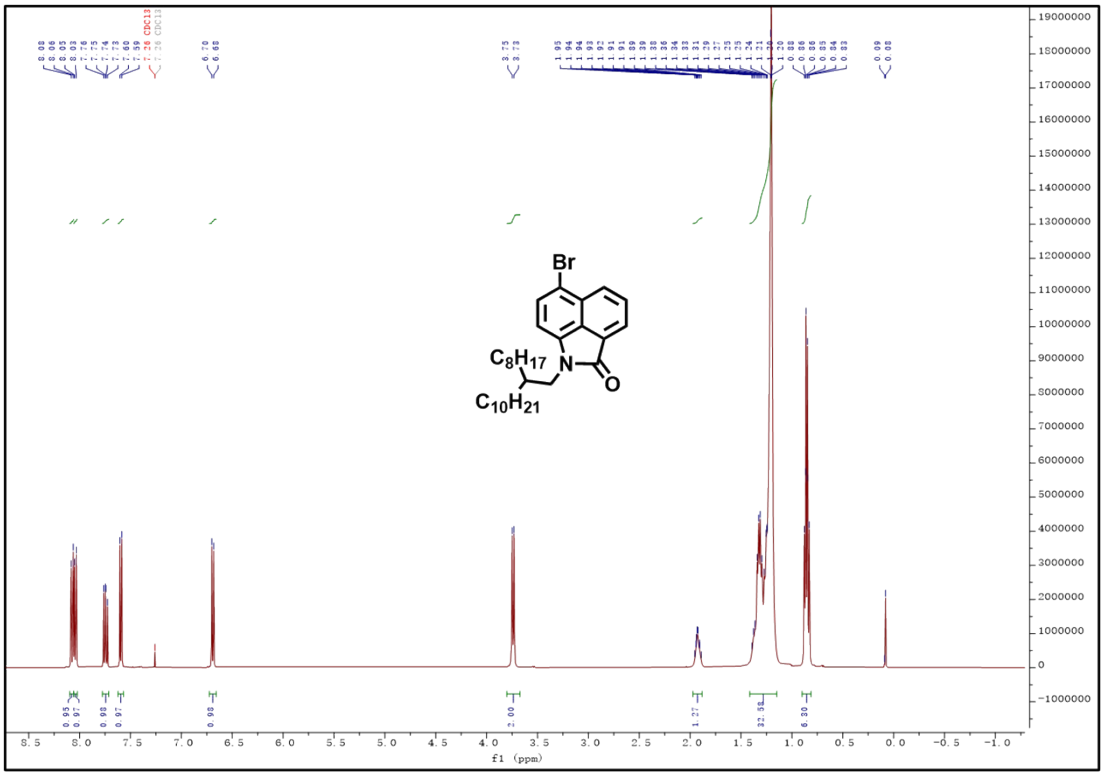

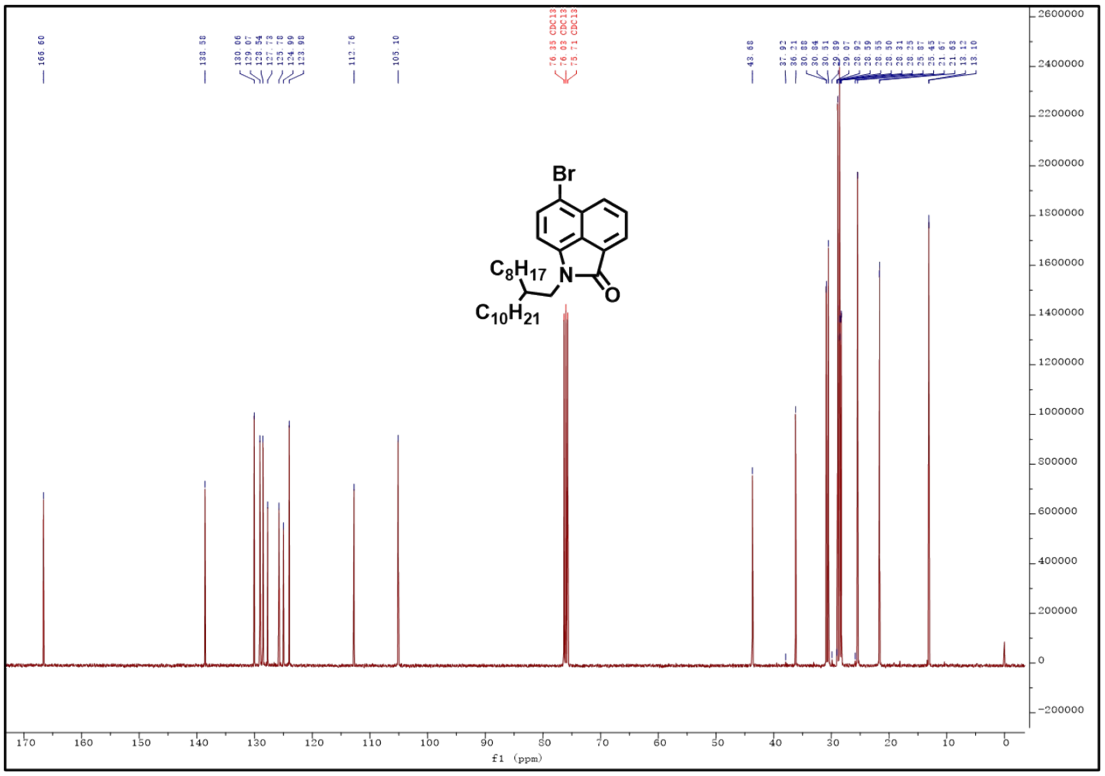

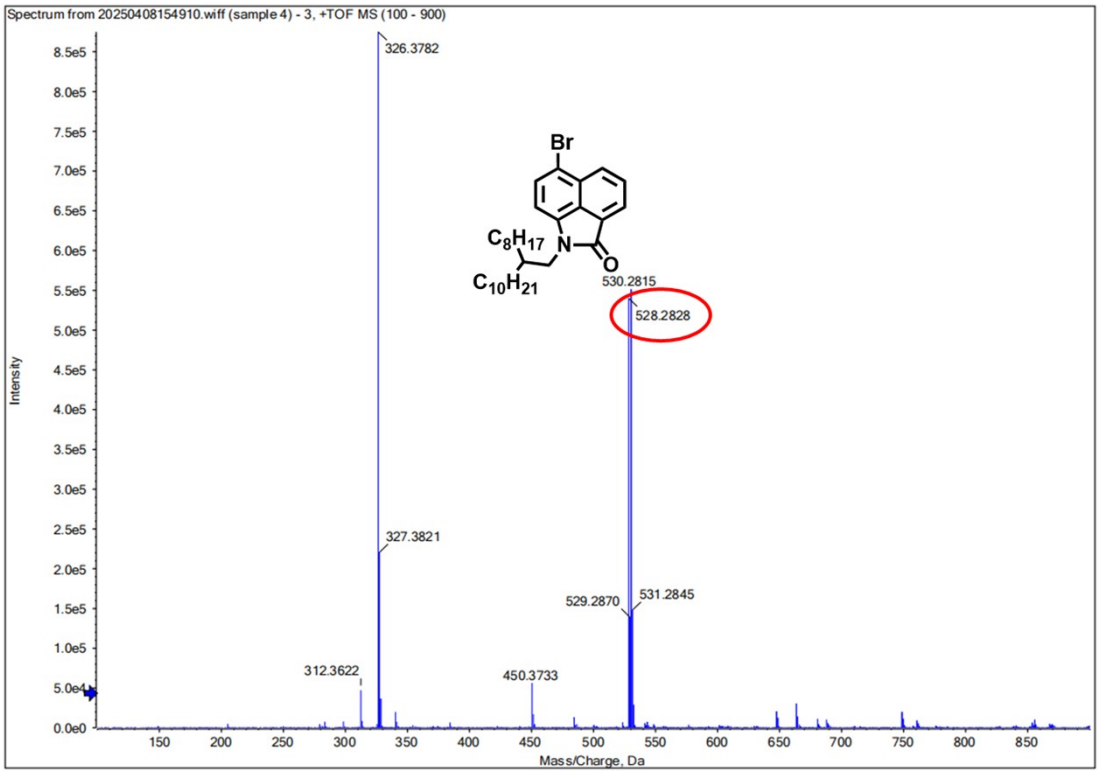

Figure S3. ^{1}H NMR, ^{13}C NMR, and TOF-MS spectra of compound 3.

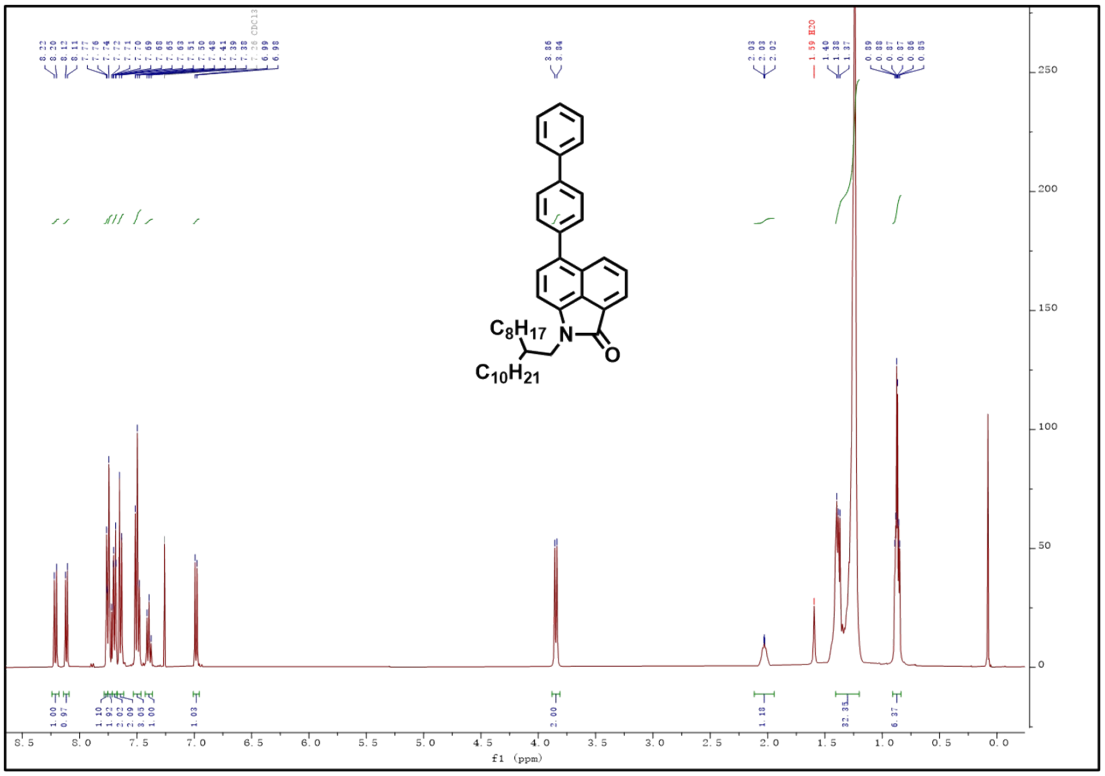
C8H17
N
O
C10H21
f1 (ppm)

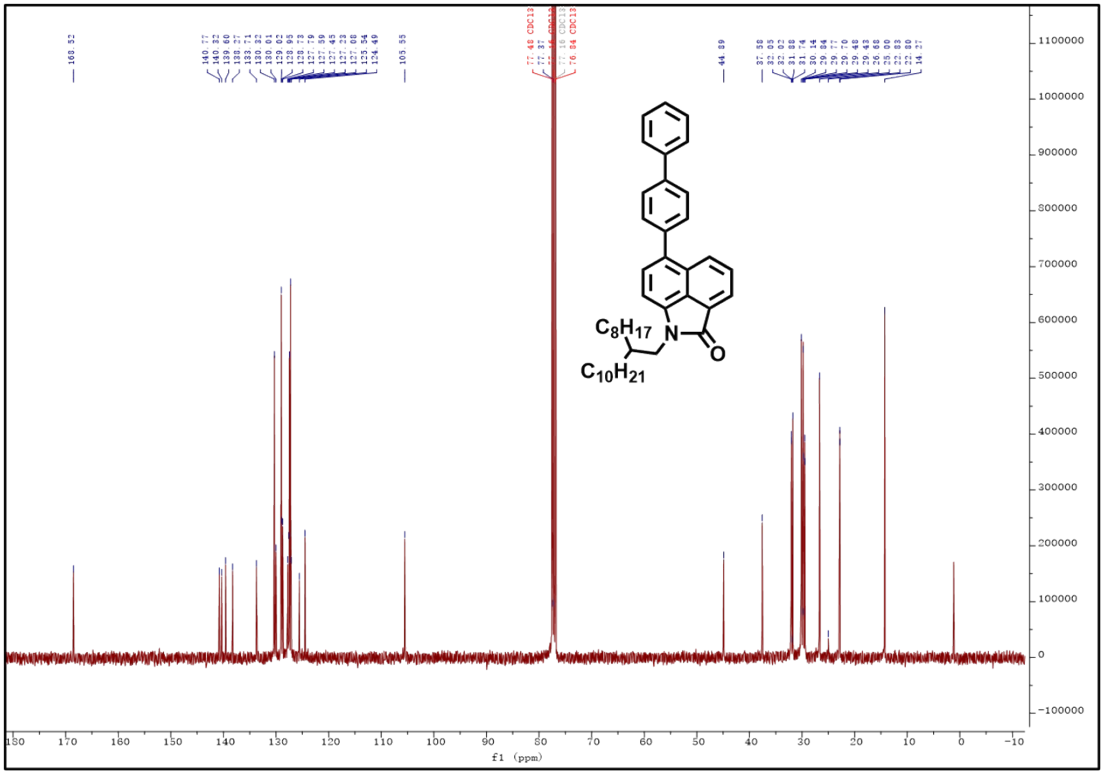
C8H17
N
O
C10H21
f1 (ppm)

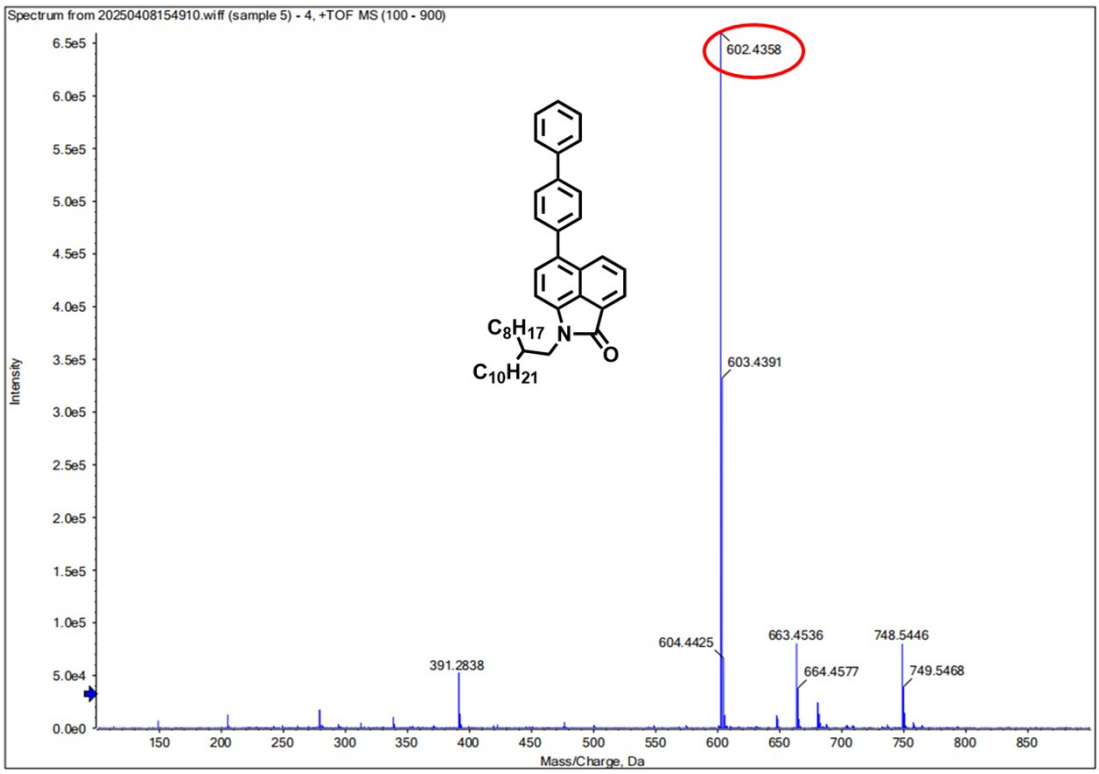

Figure S4. ^{1}H NMR, ^{13}C NMR, and TOF-MS spectra of compound 4.

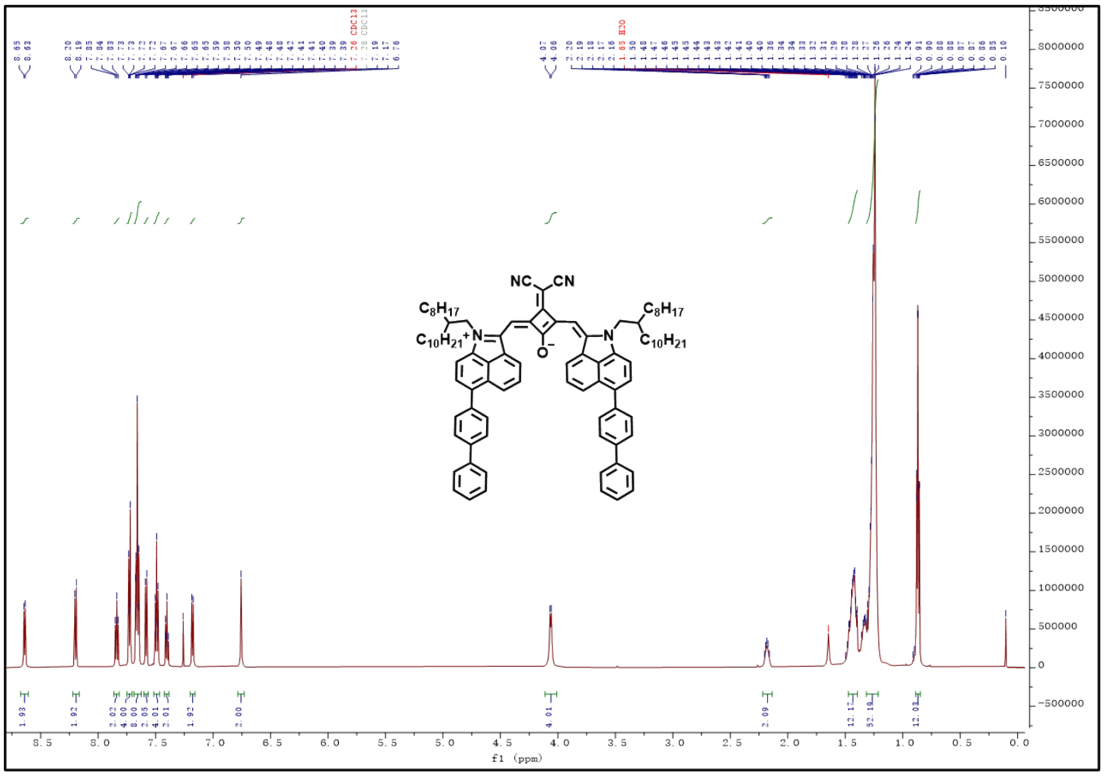

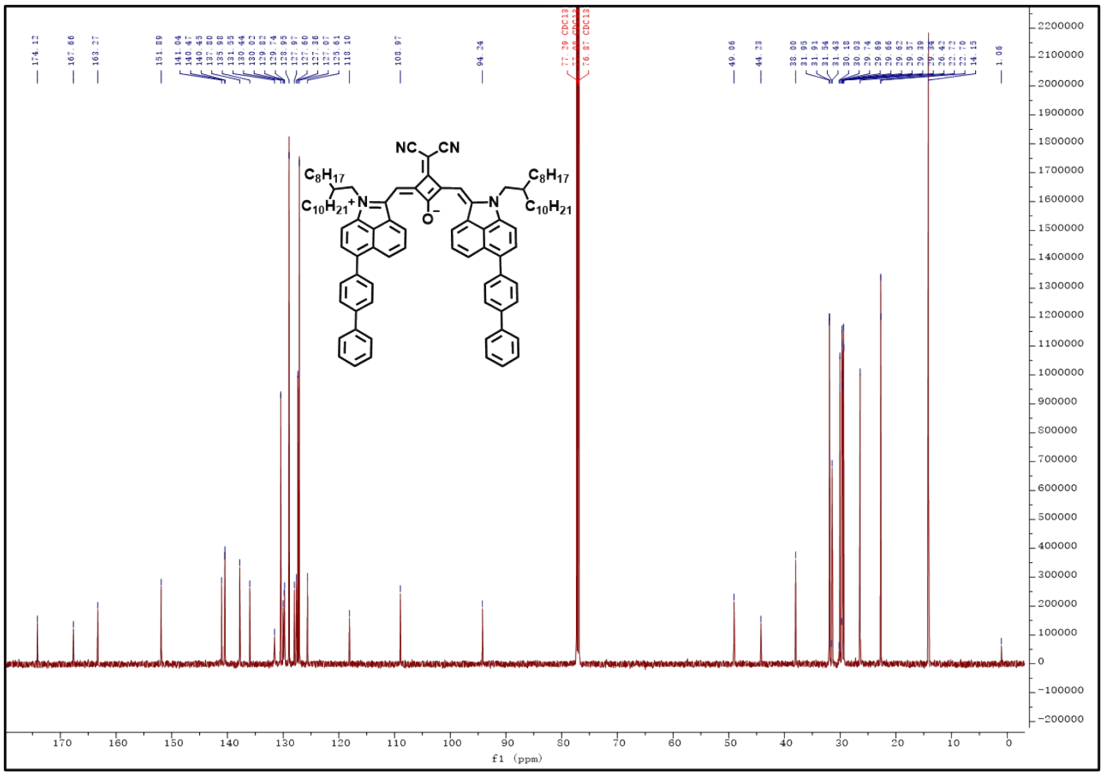

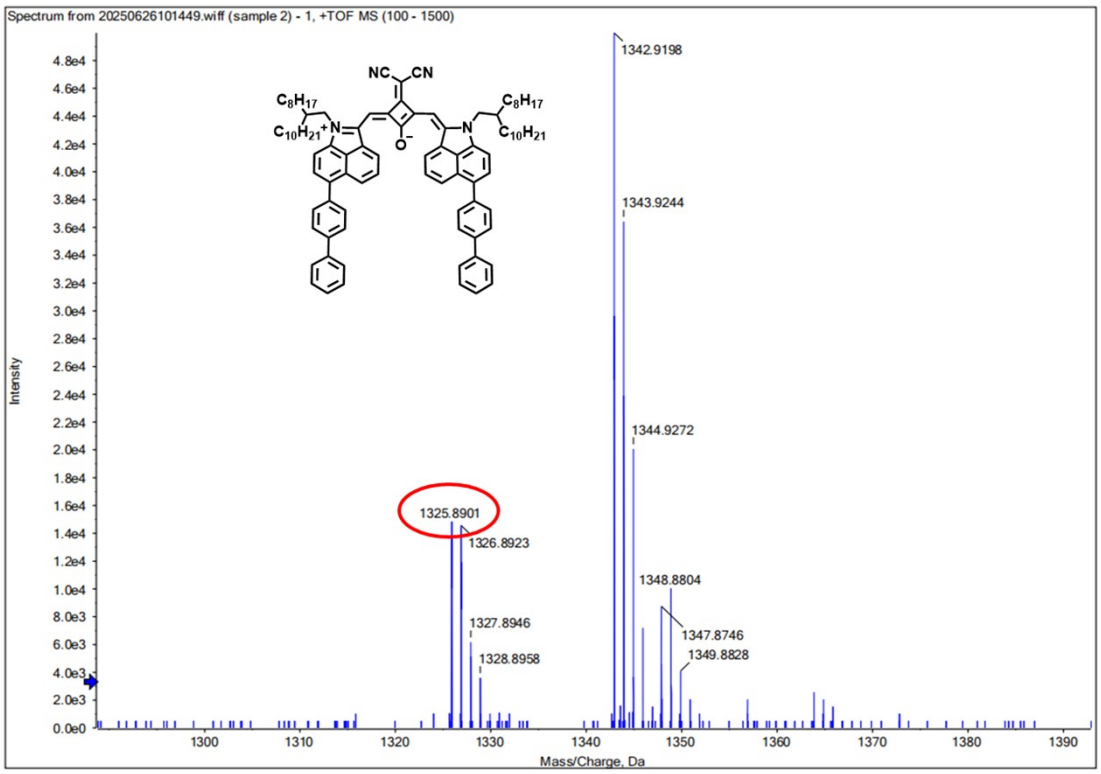

Figure S5. ^{1}H NMR, ^{13}C NMR, and TOF-MS spectra of compound 6 (SQ-BiPh).

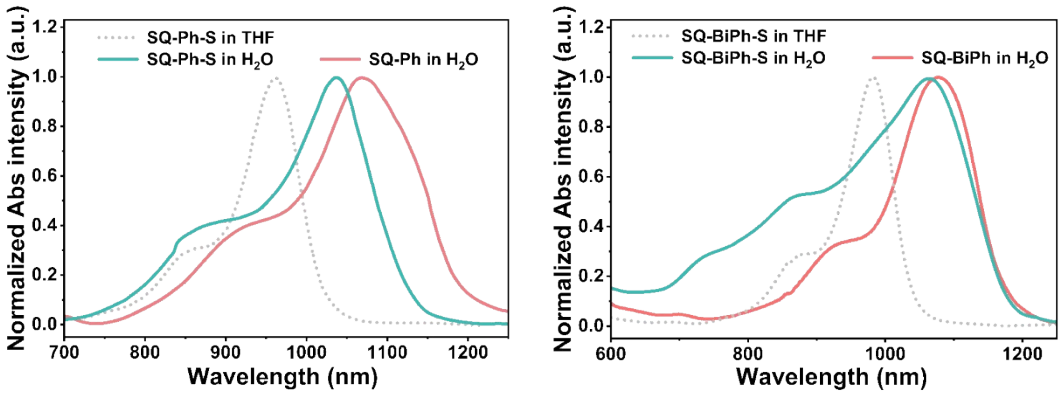

Figure S6. Absorption spectra of SQ-Ph-S and SQ-BiPh-S aggregates in H_2O (fw=100%) and in THF at room temperature, and absorption spectra of SQ-Ph and SQ-BiPh in H_2O (fw=100%), recorded at room temperature.

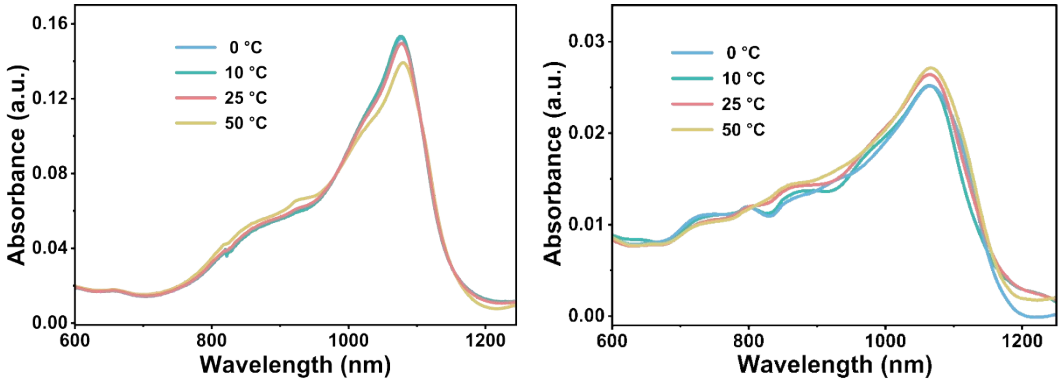

Figure S7. Absorption spectra of SQ-Ph-S and SQ-BiPh-S aggregates in H_2O (fw = 100%) recorded at different temperatures.

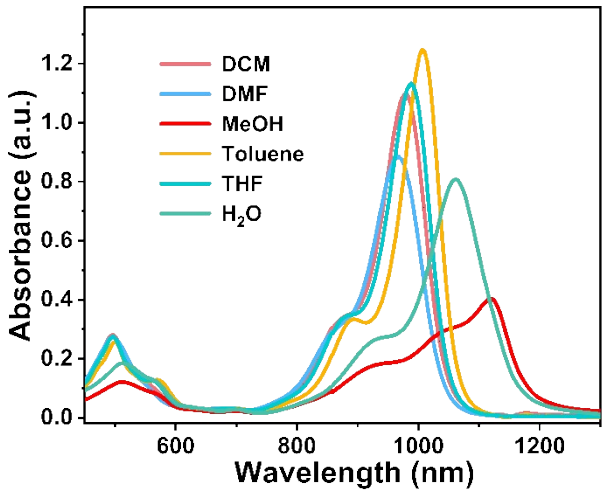

Figure S8. Absorption spectra of SQ-BiPh in different solvents.

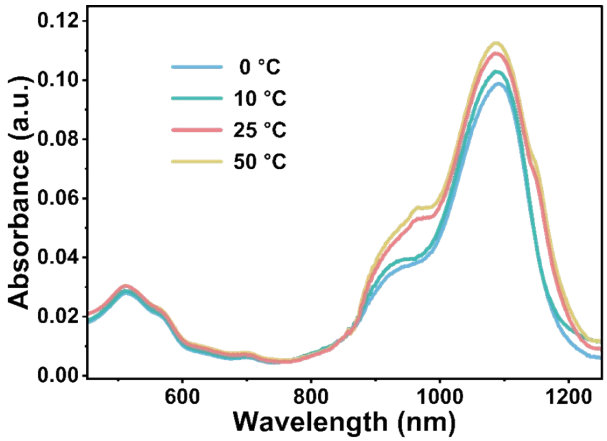

Figure S9. Absorption spectra of SQ-BiPh aggregates in H_2O (fw = 100%) recorded at different temperatures.

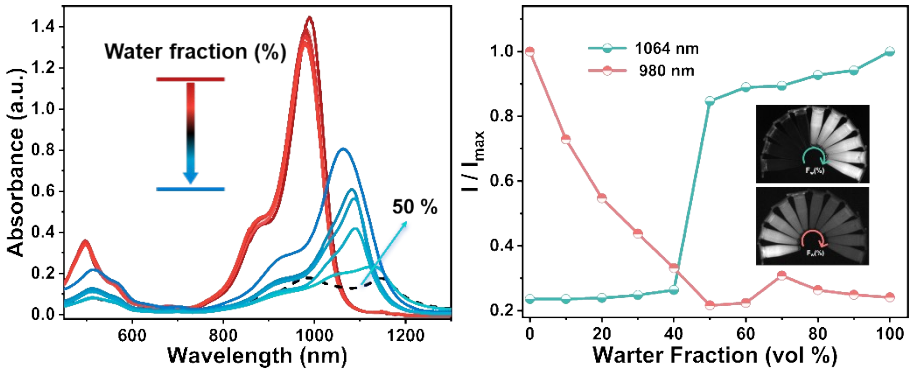

Figure S10. Absorption spectra and the relative photoluminescence intensity (I/Imax) of SQ-BiPh in THF/H_2O mixtures as a function of water fraction. Fluorescence imaging conditions: excitation at 980 nm and 1064 nm with corresponding long-pass filters, laser power density 0.3 W/cm^2, exposure time 100 ms.

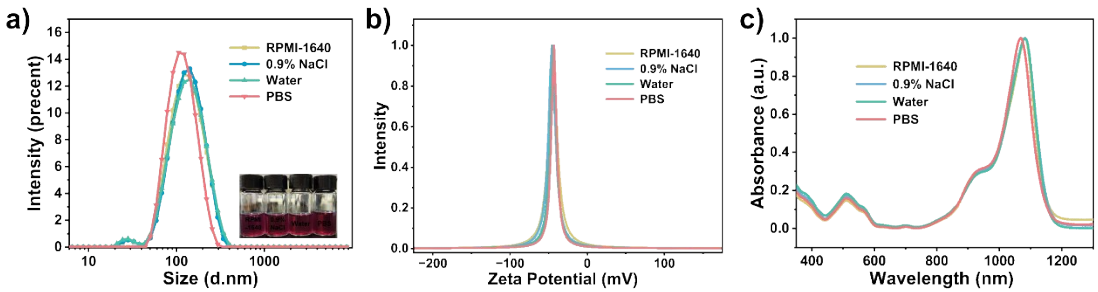

Figure S11. Particle size, zeta potential, and UV-vis absorption spectra of SQ-BiPh NPs in various physiological media (PBS, pH 7.4; 0.9% NaCl; water and RPMI-1640).

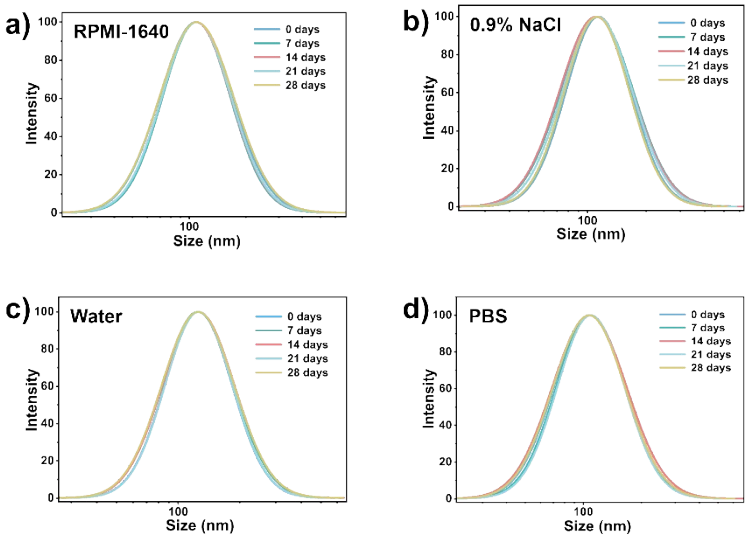

Figure S12. Particle size distribution of SQ-BiPh NPs in different physiological media after storage at 4 °C for one month.

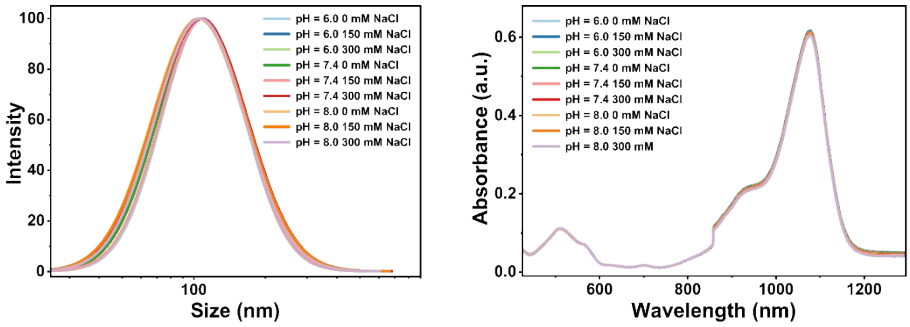

Figure S13. Particle size and UV-vis absorption spectra of SQ-BiPh NPs under different pH conditions and ionic strengths.

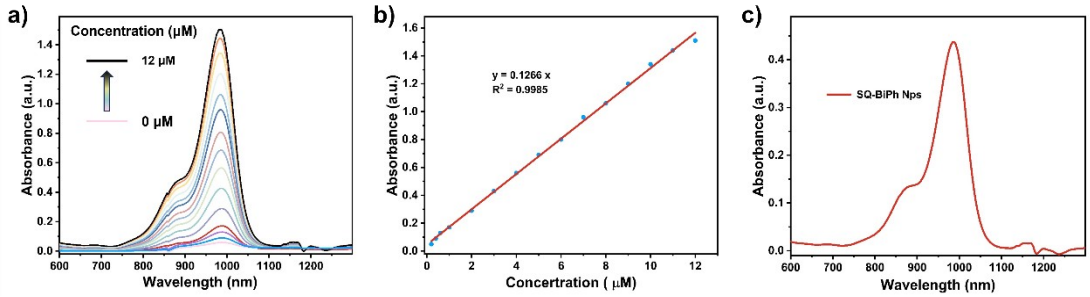

Figure S14. a) and b) show the standard curve depicting the relationship between SQ-BiPh concentration and absorbance. Figure c) shows the absorbance of SQ-BiPh in the tested SQ-BiPh@NPs after disruption with THF solvent.

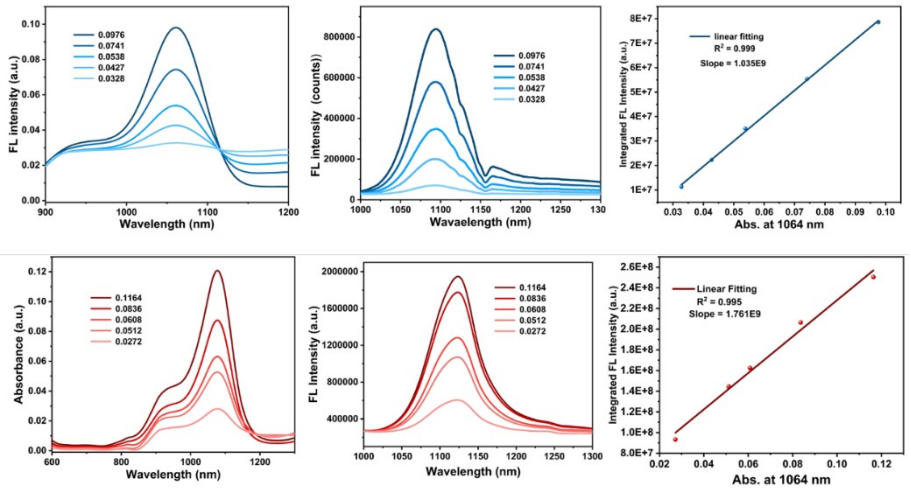

Figure S15. UV-vis absorption spectra of IR1061 and SQ-BiPh NPs with optical density (OD) values at 1064 nm. Fluorescence spectra of IR1061 and SQ-BiPh NPs with integrated NIR-II fluorescence intensities from 1000-1300 nm.

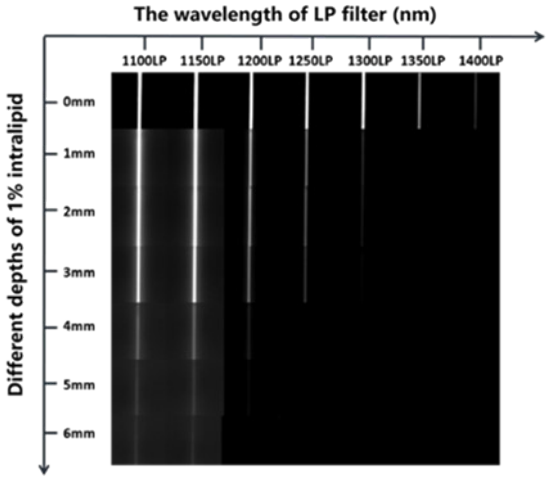

Figure S16. Penetration depth imaging of SQ-BiPh NPs in a fat emulsion solution. The imaging conditions were set as follows: excitation was performed at 1064 nm with a laser power density of 0.3 W/cm^2 and an exposure time of 100 ms. The configuration of the filters is shown in the figure.

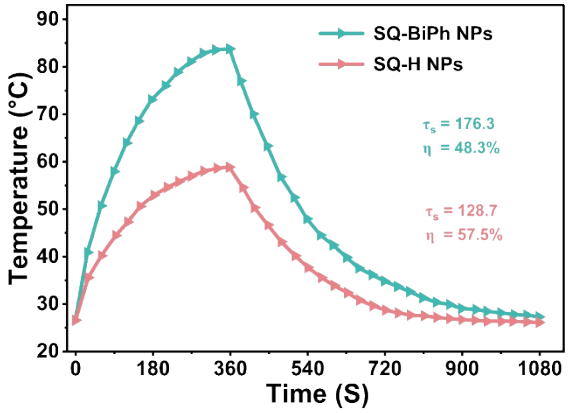

Figure S17. Comparison of photothermal performance of SQ-H NPs (60 μM, 0.15 mL) and SQ-Ph NPs (60 μM, 0.15 mL) under 1064 nm laser irradiation (1.0 W cm^{-2}), respectively.

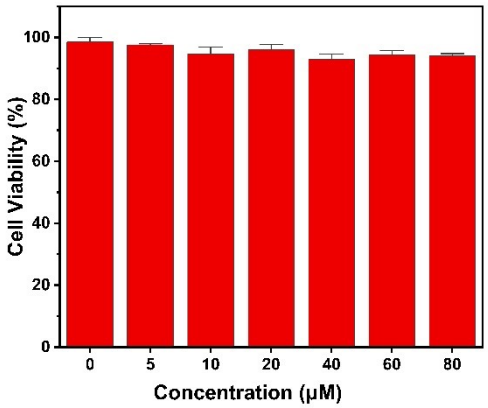

Figure S18. Cell viability of HUVEC treated with SQ-BiPh NPs at different concentrations.

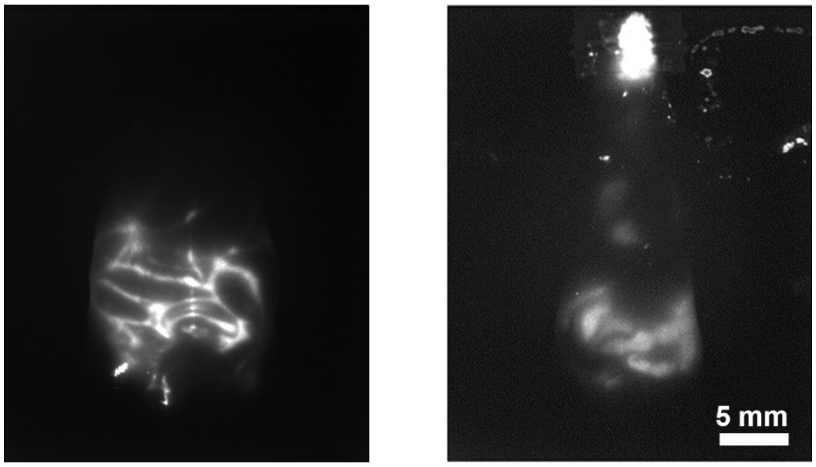

Figure S19. Fluorescence imaging of mice following intraperitoneal (i.p.) injection and oral gavage administration. The imaging conditions were set as follows: 1064 nm excitation, laser power density of 0.3 W/cm^2, a 1064 nm long-pass filter combined with a 1350 nm filter, and an exposure time of 100 ms. The injection concentration was 200 μM, with a volume of 200 μL.

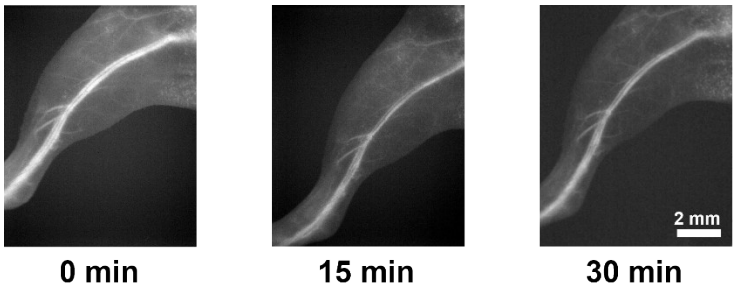

Figure S20. NIR-II fluorescence images of the left hindlimb during the treatment process.

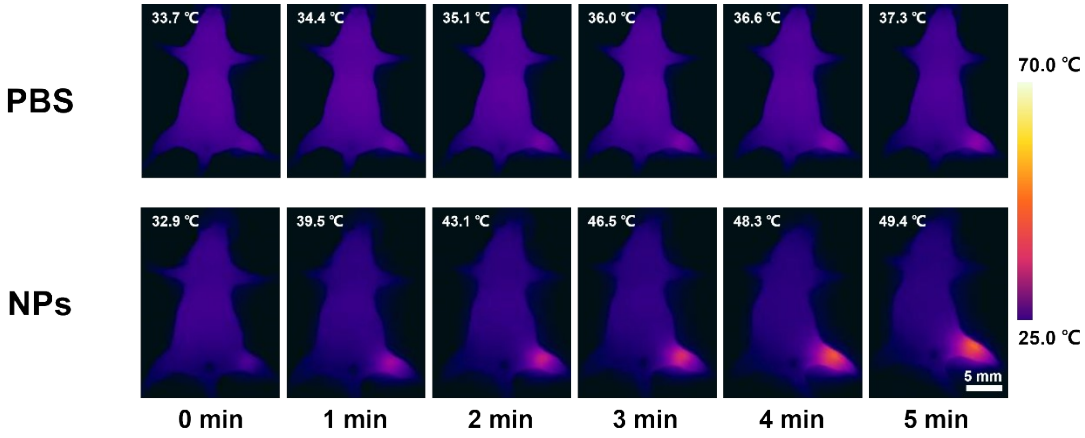

Figure S21. Infrared thermal images of thrombotic leg veins treated with PBS and SQ-BiPh NPs under 1064 nm laser irradiation (0.5 W/cm², 5 minutes). Scale bar = 5 mm.

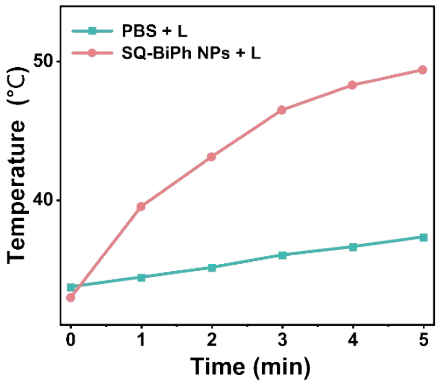

Figure S22. The corresponding photothermal heating curves.

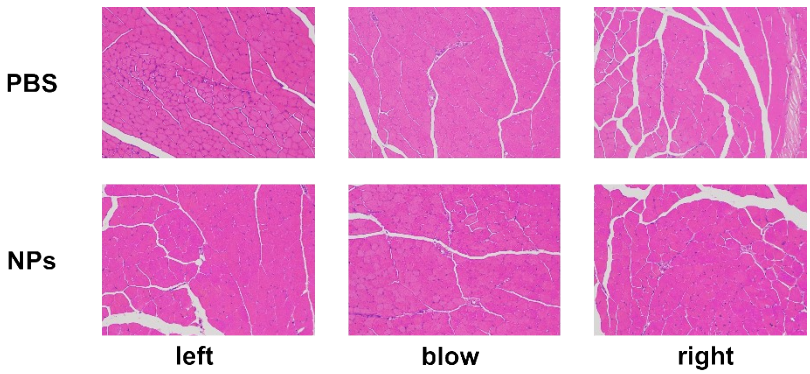

Figure S23. H&E staining of tissues adjacent to the thrombus site in different treatment groups.

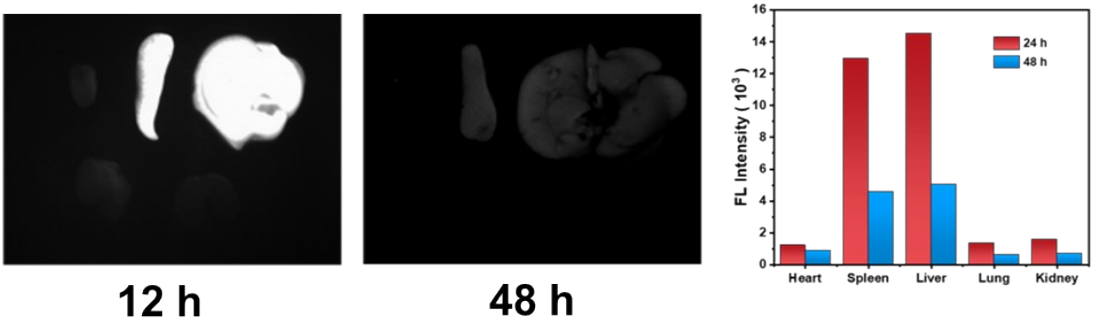

Figure S24. 12 h and 48 h post-injection, along with the corresponding fluorescence intensity profiles of major organs and tumor sites. The imaging conditions were set as follows: 1064 nm excitation, laser power density of 0.3 W/cm^2, a 1064 nm long-pass filter, and an exposure time of 100 ms.

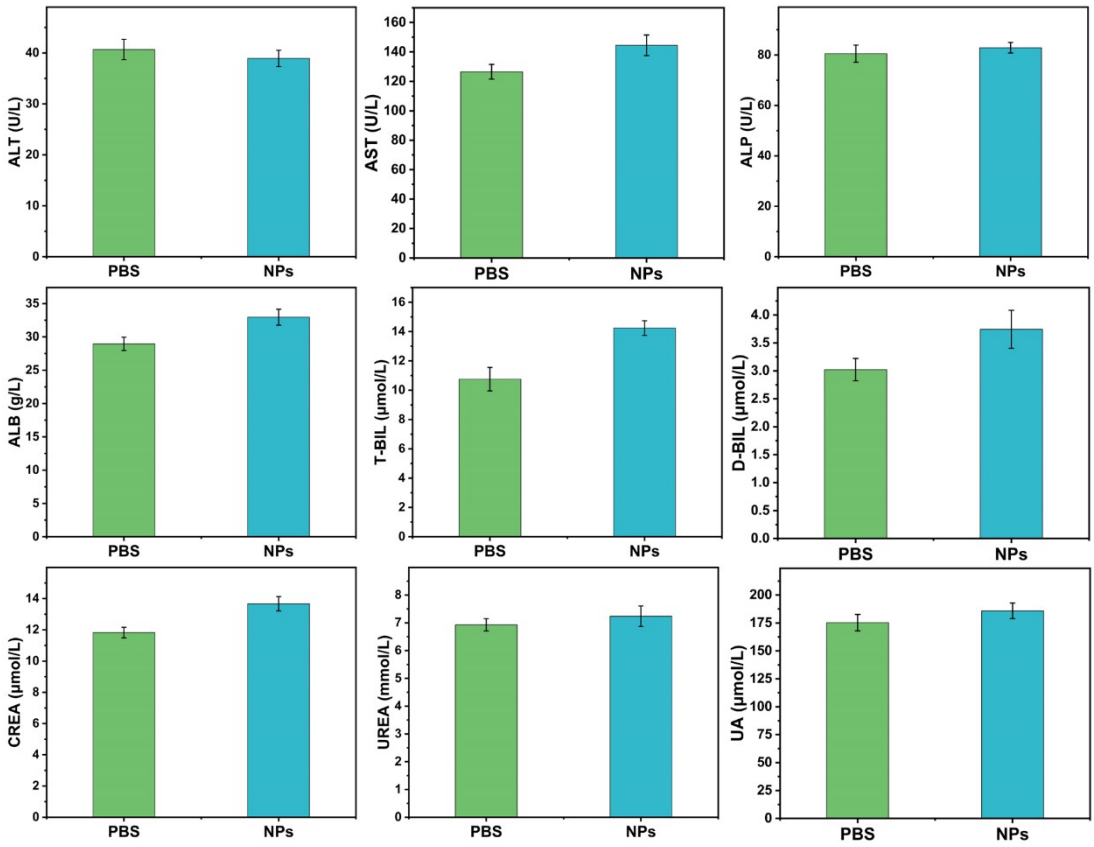

Figure S25. Blood biochemistry results of mice after tail vein injection of PBS or SQ-BiPh NPs (200 μL, 80 μM) for 14 days.

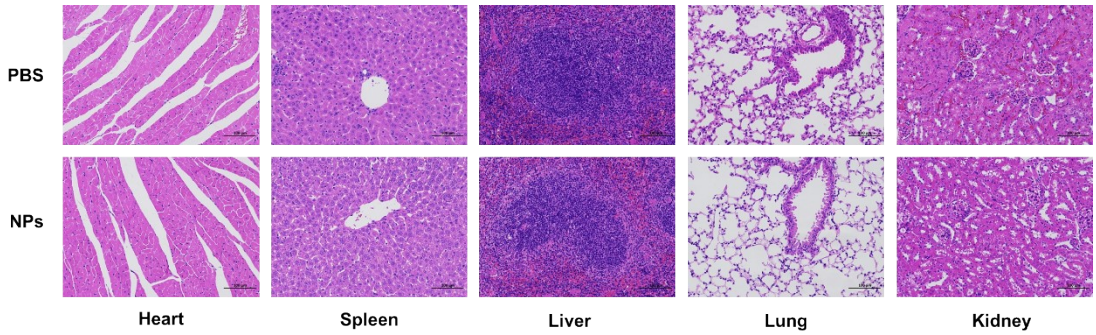

Figure S26. Major organ histology (H&E stained) of healthy BALB/c mice without treatment (PBS group) and after systemic administration of SQ-BiPh NPs (200 μL, 80 μM) for 14 days. Scale bar: 100 μm.

Reference

[1]. Y. Wang, G. Xia, M. Tan, M. Wang, Y. Li and H. Wang, Adv. Funct. Mater., 2022, 32, 2113098.

[2]. L. Si, G. Xia, G. Zhang, W. Xu, F. Zhou, X. Song, H. Wang and H. Wang, ACS Appl. Mater. Interfaces, 2025, 17, 41586.

[3]. H. Shen, F. Sun, X. Zhu, J. Zhang, X. Ou, J. Zhang, C. Xu, H. H. Y. Sung, I. D. Williams, S. Chen, R. T. K. Kwok, J. W. Y. Lam, J. Sun, F. Zhang and B. Z. Tang, J. Am. Chem. Soc., 2022, 144, 15391.

[4]. Y. Wan, Y. Gao, W.-C. Wei, K.-W. Lee, J.-H. Tan, C.-Y. Chen, H. Chen, S. Li, K.-T. Wong and C.-S. Lee, ACS Nano, 2024, 18, 27949.

[5]. M. Liu, H. Tan, B. B. Chen, C. Lu, B. Wu, Y. Zhu, R. Zhang, Z. Tian, Y. Luo, Z. Zhao and B. Z. Tang, ACS Nano, 2025, 19, 41586.

[6]. H. Wang, C. Tang, Y. Xiang, C. Zou, J. Hu, G. Yang and W. Zhou, J. Nanobiotechnol., 2024, 22, 146.

[7]. D. Zhou, G. Zhang, J. Li, Z. Zhuang, P. Shen, X. Fu, L. Wang, J. Qian, A. Qin and B. Z. Tang, ACS Nano, 2024, 18, 25144.

[8]. J. Song, X. Kang, L. Wang, D. Ding, D. Kong, W. Li and J. Qi, Nat. Commun., 2023, 14, 6881.

[9]. J. Tang, L. Si, Y. Wang, G. Xia and H. Wang, Adv. Healthcare Mater., 2025, 14, 2404322.

[10]. Y. Ye, Z. Chen, S. Zhang, P. Slezak, F. Lu, R. Xie, D. Lee, G. Lan and E. Hu, Research, 2024, 7, 0388.

[11]. D. Zhou, J. Tong, L. Zhang, Y. Yao, Y. Gao, Y.-c. Wang, G. Xu, G. Shan, L. Ren and B. Z. Tang, Biomaterials, 2026, 326, 123693.

[12]. X. Meng, J. Song, Z. Du, Y. Tao and J. Qi, ACS Nano, 2025, 19, 10323.

[13]. X. Zheng, H. Li, S. Gao, K. Mullen, J. Zhang, C. Ji and M. Yin, Small, 2024, 20, 2403284.